Heliyon 10 (2024) e40267

Contents lists available at ScienceDirect

Heliyon

journal homepage: www.cell.com/heliyon

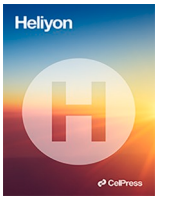

Research article

Identification of PANoptosis-based signature for predicting the prognosis and immunotherapy response in AML

Lu Zhang [a,b,1], Yanan Yu [a,b,1], Guiqing Li [a,1], Jiachun Li [c], Xiaolin Ma [a], Jiao Ren [a,b], Na Liu [a,b], Songyue Guo [a,b], Jiaqiu Li [a,b,**], Jinwei Cai [d,*]

[a] Department of Oncology, Affiliated Hospital of Shandong Second Medical University, School of Clinical Medicine, Shandong Second Medical University, Weifang, Shandong, 261053, China
[b] Clinical Research Center, Affiliated Hospital of Shandong Second Medical University, Weifang, Shandong, 261031, China
[c] Department of Information Engineering, Weifang Vocational College of Food Science and Technology, Weifang, 262100, Shandong, China
[d] Department of Oncology, People's Hospital of Kecheng District, Quzhou, 324000, Zhejiang, China

ARTICLE INFO

Keywords:
Acute myeloid leukemia
PANoptosis
Prognostic model
Immunotherapy efficacy
Single-cell RNA sequencing
Drug sensitivity

ABSTRACT

Background: In recent years, the incidence of acute myeloid leukemia (AML) has increased rapidly with a suboptimal prognosis. In AML, cell death is independent of tumorigenesis, tumor invasion, and drug resistance. PANoptosis is a newly discovered form of cell death that combines pyroptosis, apoptosis, and necroptosis. However, no studies have explored the role of PANoptosis-based signatures in AML.

Methods: We screened for PANoptosis-related genes and established a PANoptosis-risk signature using the least absolute shrinkage and selection operator (LASSO) and Cox regression analysis. We combined TCGA, bulk RNA sequencing, and single-cell sequencing to investigate the correlation between candidate genes and the AML tumor microenvironment.

Results: The PANoptosis risk signature effectively predicted prognosis with good sensitivity and specificity. The risk score emerged as an independent prognostic factor. Functional enrichment analysis of PANoptosis-related differentially expressed genes suggested that the risk score may be related to cell immunity. Patients with high-risk scores exhibited increased immune cell infiltration, implying a hot tumor immune microenvironment. The risk score was positively correlated with the immune scores and expression levels of immune checkpoints. Therefore, we identified three model factors, BIRC3, PELI1, and PRKACG, as predictors for immunotherapy efficacy. Single-cell sequencing analysis demonstrated that PELI1 and BIRC3 may participate in the regulation of the AML immune microenvironment. Finally, we performed a drug sensitivity analysis to target BIRC3 and PELI1 using molecular docking and molecular dynamics simulations.

Conclusion: Our study established and verified a PANoptosis risk signature to predict the survival and immunological treatment response in AML.

* Corresponding author.
** Corresponding author. Department of Oncology, Affiliated Hospital of Shandong Second Medical University, School of Clinical Medicine, Shandong Second Medical University, Weifang, Shandong, 261053, China.
E-mail addresses: lijq@sdsmu.edu.cn (J. Li), imvp16@163.com (J. Cai).
[1] These authors contributed equally: Lu Zhang, Yanan Yu and Guiqing Li.

https://doi.org/10.1016/j.heliyon.2024.e40267
Received 21 March 2024; Received in revised form 21 September 2024; Accepted 7 November 2024
Available online 8 November 2024

1. Introduction

Similar to many other malignant tumors, acute myeloid leukemia (AML) primarily results from genetic variations, including chromosomal translocations and gene mutations [1,2]. These alterations lead to malignant transformation of hematopoietic stem cells (HSCs) and impaired hematopoiesis. An increasing number of pathogenic genetic variations have been identified that participate in multiple processes, such as hematopoietic differentiation, the cell cycle, apoptosis, and DNA repair [1,3]. For example, RUNX plays a crucial role in the initiation of hematopoiesis, and the disruption of its normal structure can inhibit the transcription of PU.1, resulting in functional defects in HSCs [4]. Additionally, genetic defects in RIPK3 have been observed in some patients with AML, which inhibit tumor necrosis factor-mediated cell death, leading to the accumulation of leukemia cells at disease onset and the promotion of disease progression [5]. High rates of relapse and widespread drug resistance in AML are attributed to complex genetic mutations, particularly in elderly patients [6]. Similar to other tumors, high heterogeneity is a characteristic feature of AML. Owing to the high heterogeneity, individualized therapies, such as more accurate immunotherapy and targeted therapy, have been advocated in numerous studies on AML [7].

Abnormalities in the cell death pathway are crucial factors that allow tumor cells to acquire immortal characteristics. Rectifying disordered cell death pathways is essential for normal biological processes, including the elimination of genetically mutated cells to prevent cancer, eradicating pathogenic bacteria to prevent infectious diseases, and renewing aging cells, among other functions. Therefore, it is important to explore the role of cell death and its underlying mechanisms in cancer treatment. By summarizing previous experiments, we found several FDA-approved targeted agents related to programmed cell death (PCD) in recent research over the past decade [8,9]. PCD is characterized by pyroptosis, apoptosis, and necroptosis. In recent years, many studies have identified proteins involved in pyroptosis and apoptosis as candidate targets for reliable and effective agents with low toxicity and high selectivity [10,11]. In 2018, venetoclax received accelerated approval for use in adults by selectively targeting BCL-2 and activating apoptosis. In similar experiments, traditional chemotherapy combined with novel targeted agents improved the therapeutic index of AML because of the enhanced function of Ara-C in inducing cell cycle arrest and necrosis [12]. Early drug resistance is generally caused by chemotherapy-resistant leukemia stem cells (LSCs) within the protective bone marrow microenvironment. The sensitivity of LSCs to AML first-line therapies remains poorly understood in current research, presenting a challenging yet meaningful entry point for addressing AML recurrence and drug resistance [13]. The BRD4 degrader, dBET 6, targets BRD4 and inhibits anti-apoptotic mechanisms in AML cells. When combined with gilteritinib, venetoclax, or ARA-C, it synergistically induces apoptosis in LSCs and overcomes drug resistance in AML-LSCs [14]. Late drug resistance in AML is primarily due to the accumulation of re-edited key pathways, which gradually increases the intrinsic drug resistance of cells [15]. Research has shown that NRAS mutations cannot be ignored in the late resistance of patients with AML to gefitinib, and these mutations are frequently observed in late gefitinib-resistant MOLM14 and MV4 cell lines [16]. NRAS mutations accumulate progressively during the development of resistance, with a low variant allele frequency (VAF) observed in MOLM14 parental cells. Furthermore, high expression levels of FLOT1 are associated with poor prognosis in AML patients, and in vitro experiments have demonstrated that FLOT1 promotes apoptosis and pyroptosis in AML cells [10]. However, the specific regulatory mechanisms remain unclear. A detailed clinical classification of patients with AML along with a deeper and more accurate analysis of the abnormal molecular mechanisms underlying the onset and resistance to AML is essential to identify and develop more effective and less harmful treatment strategies.

PANoptosis, a newly identified form of cell death, involves a lytic and inflammatory cell death pathway [17–19]. PANoptosis is regulated by the PANoptosome, a cytoplasmic protein complex that simultaneously incorporates structural features and proteins that are characteristic of pyroptosis, apoptosis, and necroptosis. Given that pyroptosis, apoptosis, and necroptosis are all inhibited in leukemia [20–23], they also play critical roles in the tumorigenesis and progression of AML. To investigate this, we established a model to assess the biological significance of PANoptosis in AML patients.

2. Materials and methods

2.1. Clinical data collection

RNA expression and clinical data of AML patients were obtained from The Cancer Genome Atlas (TCGA) database. Patients lacking the corresponding clinical information were excluded. A total of 141 patients with AML with complete clinical information were included in the subsequent analysis. Raw microarray datasets, GSE37642 and GSE12417, were retrieved from The Gene Expression Omnibus (GEO) database. In the above RNA sequencing data, genes with expression > “0” were retained, whereas poorly expressed genes with expression = “0” were excluded. The screened RNA sequencing data was normalized using the “Limma” package in R, and the gene expression profiles were obtained.

2.2. Searching the PANoptosis gene list

The PANoptosis gene list contained the main constituent genes of apoptosis, pyroptosis, necroptosis, and PANoptosomes. The apoptosis gene list, which included 93 genes, was obtained from GeneCards (https://www.genecards.org/) and the Kyoto Encyclopedia of Genes and Genomes (KEGG). The list of 74 pyroptosis genes was obtained from GeneCards and REACTOM. A list of 63 necroptosis genes was obtained from GeneCards and AmiGO 2. Finally, 11 PANoptosome genes were obtained from GeneCards.

2.3. Analysis of PANoptosis-related genes in AML

Through univariate Cox regression analysis calculated using the "survival" package R, 197 PANoptosis-related genes (PRGs) were selected for correlative signature construction. To explore key genes and interactions between PRGs, we used the STRING database to design an interactive network of PRGs [24]. Gene Ontology (GO) and Kyoto Encyclopedia of Genes and Genomes (KEGG) analysis was conducted to screen the biological functions of PRGs in AML using the "clusterProfiler" package in R, with $p < 0.05$.

2.4. Construction of the PANoptosis-risk signature

To avoid factor overfitting in the risk signature, the most significant candidate PRGs were identified using LASSO-penalized Cox regression analysis in the GSE37642 cohort. The "glmnet" and "survival" packages in R were used. Then, 19 candidate PRGs were selected, and multivariate stepwise Cox proportional hazards regression models were entered into the "survival" package in R. Finally, a risk-score calculation formula was developed. We calculated and obtained the risk scores for patients based on the expression of the model factors. The formula used was as follows:

risk score = Σ the corresponding coefficient (i) × the expression value of gene (i).

2.5. Validation of the predictive efficiency of the PANoptosis-risk signature

AML patients in the GSE37642 cohort were divided into two distinct groups according to their risk scores. Differences in the outcomes of patients with AML between the two groups were determined by Kaplan–Meier (K-M) survival analysis. A time-dependent receiver operating characteristic curve was used to verify the signature accuracy. Two AML cohorts were downloaded: TCGA (n = 141) and GSE12417 (n = 162). The risk scores were calculated using the PANoptosis risk signature. We further used the K-M analysis and ROC curve to verify the model.

2.6. Establishment of the Nomogram

Nomograms have great clinical application value in predicting the prognosis of patients with tumors, and their accuracy makes their application convenient and simple. With the "rms" package in R, the age and risk scores of patients were used to establish a nomogram [25] that could predict the one-, three- and five-year prognosis of AML patients. Additionally, calibration curves were generated to evaluate the value of the nomogram.

2.7. Functional enrichment analysis of PANoptosis-related differentially expressed genes

To further explore this signature, we divided AML patients from the TCGA cohort into high- and low-risk groups. Then, we identified PANoptosis-related differentially expressed genes (PRDEGs) between the two groups ($|\log_2 FC > 1|$, $p < 0.05$) by using the "limma" package in R. Representative biological processes and signaling pathways of PRDEGs were sought by GO and KEGG analysis using the "clusterProfiler" package in R. To thoroughly investigate and increase the credibility of results from GO and KEGG analysis, we conducted GSEA analysis using the "GSVA" package in R.

2.8. Evaluation of immune cell infiltration in the AML tumor microenvironment

Multiple algorithms (xCell, TIMER, EPIC, and MCPcounter) were performed to evaluate the abundances of immune cell infiltration using the "IOBR" package in R. We obtained and selected immune related genes to calculate the Pearson correlation between the immune cells and the expression levels of risk genes using the "corrplot" package in R. The correlations between immune scores and the expression of model factors were obtained and displayed using the "ggplot2" package in R. We combined the gene expression profiles to evaluate the degree of immune cell infiltration in the two groups using ssGSEA, with $p < 0.05$.

2.9. Predicting the immunotherapy efficacy using risk genes

We used the ESTIMAT algorithm to calculate the ESTIMATE-stromal-immune scores of patients with AML and compared the scores of the high- and low-risk groups to identify differences. Furthermore, immune checkpoint gene expression was compared with the risk score. Statistical significance was set at $p < 0.05$. In the GSE37642 cohort, we conducted a K-M analysis of risk genes with excellent performance using the "survival" package in R. Most importantly, we calculated the Tumor Immune Dysfunction and Exclusion (TIDE) scores for the TCGA cohort using the TIDE database [26].

2.10. Single-cell sequencing analysis

To explore the distribution of model factors in the AML tumor microenvironment, we used the GSE116256 dataset from the GEO

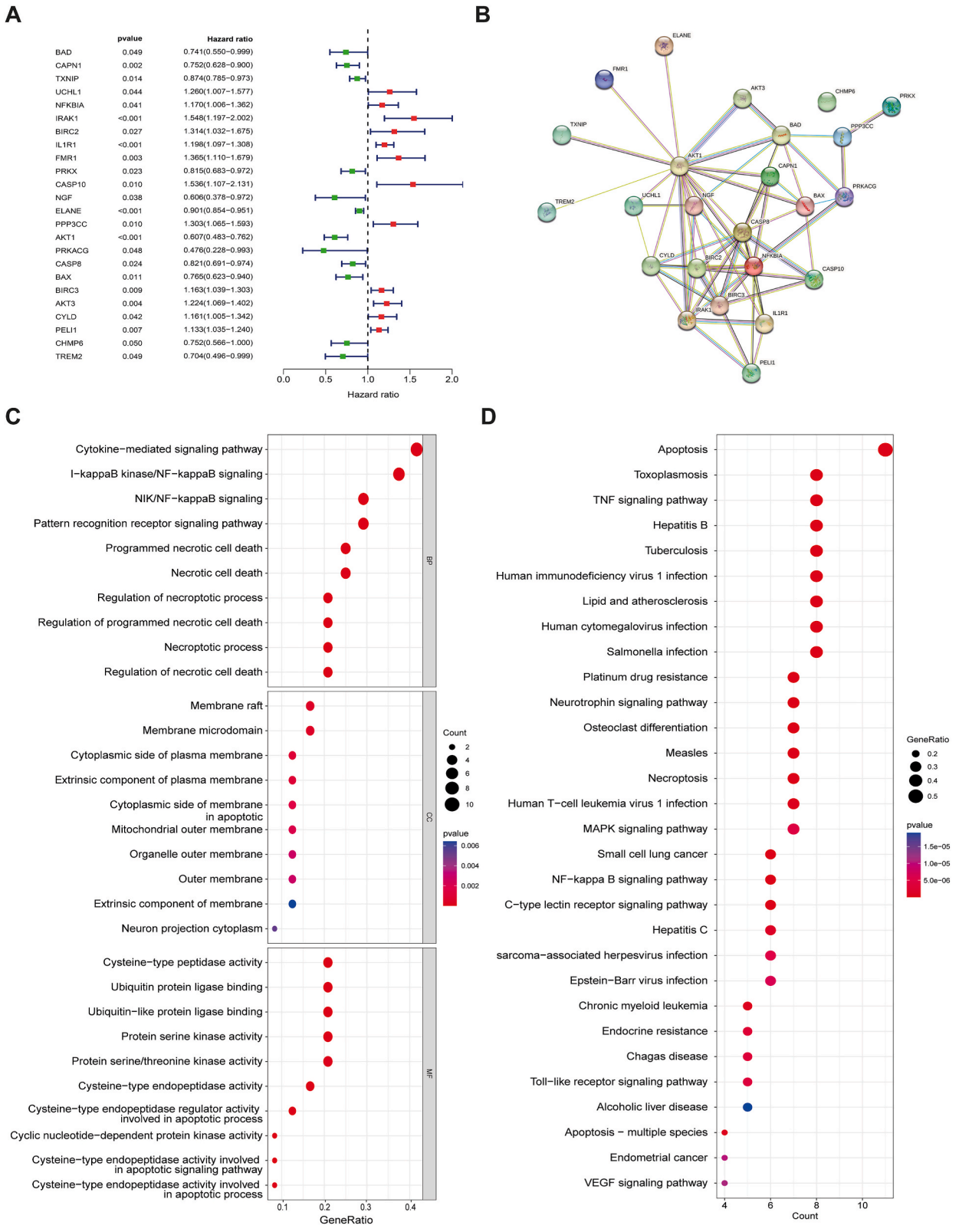

Fig. 1. Screening and GO, KEGG analysis of PANoptosis-related genes (PRGs) in AML. (A) Univariate Cox regression analysis of PRGs in AML using GSE37642 cohort. (B) Interactive networks among the 24 PRGs. (C–D) GO and KEGG analysis of PRGs in AML.

database. We obtained the GSE116256 dataset and categorized patients into three groups: confirmed AML patient group (AML), chemotherapy-induced AML patient group (AML_treat), and normal group (normal). We then analyzed gene expression in bone marrow samples from these different groups across various cell clusters. The samples from AML patients were processed and clustered according to their cell types to calculate the characteristic expression of model factors in the AML tumor microenvironment using the "seurat" package in R. Furthermore, we used the "clusterProfiler" package in R for GO analysis of four sensitive genes obtained from single cell sequencing data analysis and visualized them by Sangerbox.

2.11. Screening of susceptible drugs

In this study, we screened the model factors and identified two risk genes. Based on these two genes, we screened out a variety of drugs by their IC50 and correlation coefficient ($IC50_{max}$ <50 and $p < 0.05$) from the Genomics of Drug Sensitivity in Cancer (GDSC) database using the "oncopredict" package in R. Subsequently, we collected the 3D structure of the BIRC3 protein (PDB ID: 2UVL) from The Protein Data Bank (PDB) and obtained the 3D structure of the PELI1 protein (AlphaFoldDB ID: Q96FA3) from the AlphaFold Protein Structure Database. Drug structures were obtained from PubChem BioAssay (PubChem) and Universal Protein Resource (Uniprot). AutoDock software was used to dock the target proteins with drugs to predict the efficacy of candidate drugs. The results are displayed as 2D and 3D structures using PyMol and LigPlot software. To further investigate the stability of the six selected compounds in binding to target proteins, we conducted 100 ns molecular dynamics simulations (MDS) on these compounds and proteins. The docking results from AutoDock served as the initial template for MDS in Schrödinger (2021–2022). We observed the degree of change in ligand and protein conformation compared to their initial states during the 100 ns simulation process. The MDS results were analyzed using 'simulation interaction diagrams.'

2.12. Statistical analysis

All statistical analyses in this study were performed using R (version 4.2.0). Univariate, multivariate, and LASSO Cox regression analyses were used to identify candidate genes in the PANoptosis-risk signature. Survival analysis was performed through K-M analysis and verified through time depended-ROC curve using the "survival," "surviviner," and "timeROC" packages in R. Correlations were calculated using Pearson and Spearman correlation tests. Differential analysis was performed using the Wilcoxon test and *t*-test. Statistical significance was set at $p < 0.05$, and $p < 0.05$, 0.01, 0.001, and 0.0001 is represented as "*", "**", "***", and "****".

3. Results

3.1. Screening of PANoptosis-related genes (PRGs) in AML

Gene expression data of 197 PRGs were retrieved from the GSE37642 cohort, and poorly expressed genes with a mean expression value of "0" were removed. We selected 160 PRGs for analysis based on their gene expression profiles. Univariate Cox regression analysis identified 24 candidate PRGs that were significantly correlated with the prognosis and outcomes of AML patients ($p < 0.05$) (Fig. 1A). The interactive networks of the 24 PRGs are shown in Fig. 1B.

3.2. GO and KEGG analysis of PRGs in AML

We explored the biological functions and signal transduction pathways of the 24 survival-related PRGs using GO and KEGG analyses. GO analysis indicated that these genes were enriched in inflammatory and cancer-related signaling pathways, such as programmed necrotic cell death, I-kappa B kinase/NF-kappa B signaling, and cytokine-mediated signaling pathways (Fig. 1C). Regarding molecular function, these genes were associated with various enzymatic activities, including cysteine-type peptidases and protein serine/threonine kinases, which are involved in cell death, and protein serine/threonine/tyrosine kinases, which are related to carcinogenicity. The results of the KEGG analysis indicated that the major pathways were related to programmed cell death pathways, such as apoptosis and necroptosis, the TNF signaling pathway, and infection by multiple pathogens (Fig. 1D).

3.3. Construction of the PANoptosis-risk signature

Through LASSO and Cox regression analyses, we selected key survival-related PRGs for modeling, and 19 genes were used in the subsequent steps (Fig. 2A and B). We then screened 10 PRGs after multivariate Cox regression analysis and calculated the coefficients of the model factors. Finally, a formula for PANoptosis-related risk scores was constructed: The risk score = UCHL1 × 0.38415 + NFKBIA × 0.19647 + CASP10 × 0.3262 + IL1R1 × 0.16132 + ELANE × (−0.11853) + AKT1 × (−0.32856) + PRKACG × (−0.85091) + BIRC3 × (−0.14324) + PELI1 × 0.08406 + TREM2 × (−0.58014). The risk scores were calculated, and patients from the three AML cohorts were divided into high- and low-risk groups based on the risk scores. K-M analysis of the GSE37642 (Fig. 2C), TCGA (Fig. 2D), and GSE12417 (Fig. 2E) cohorts revealed differences in the outcomes between patients with different risk scores. A high risk score was associated with a worse prognosis. Furthermore, the area under the time-dependent ROC curve values of the one-, three-, five-year survival predictions were 0.661, 0.751, and 0.745, respectively, in the GSE37642 cohort (Fig. 2F), 0.609 and 0.682, and 0.738, respectively, in TCGA cohort (Fig. 2G). Since the GSE12417 cohort lacked the five-year survival information of patients, we calculated the AUC values of the one-, two- and three-year survival predictions (Fig. 2H). After reviewing these results, we found that the

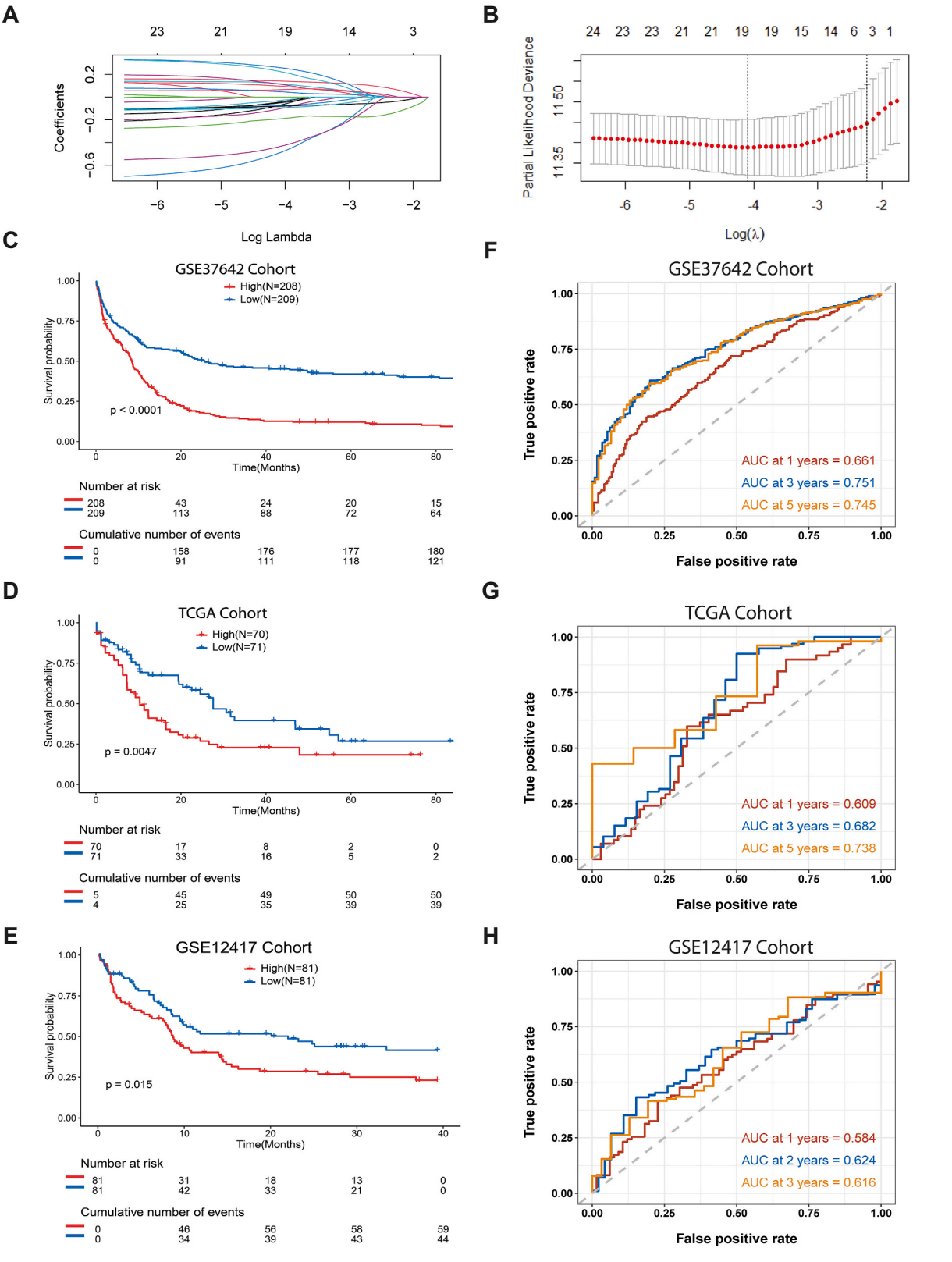

(caption on next page)

Fig. 2. Construction of the PANoptosis-risk signature. (A) The LASSO coefficient profile plot was created against the log (lambda) sequence. (B) Ten-fold cross-validation for tuning parameter (lambda) selection in the LASSO model. (C–E) Kaplan-Meier curve analysis of AML patients in GSE37642, TCGA and GSE12417 cohort by risk score. (F–H) Time-dependent ROC curves for predicting the overall survival of AML patients in GSE37642, TCGA and GSE12417 cohort.

PANoptosis risk signature predicted the prognosis of patients with AML with good sensitivity and specificity.

3.4. Comparison between clinicopathological characteristics and the PANoptosis-risk signature

Based on univariate and multivariate Cox regression analyses, the risk score of the PANoptosis-risk signature positively correlated with the survival status of patients (Fig. 3A and B), indicating that the risk score could be an independent prognostic factor for AML. The connection between model factor expression levels and clinical features is displayed using a heatmap (Fig. 3C). Further analysis revealed that this risk score could better predict the one-, three-, and five-year survival status of AML compared with other clinicopathological characteristics, such as FAB classification, age, RUNX1-RUNX1T1 fusion, and RUNX1 mutation (Fig. 3D–F). A nomogram was established to assess the conditions and outcomes of patients with AML (Fig. 4A). The calibration curves fitted the 45° line well, indicating that this risk score had a good predictive value for the one-, three-, and five-year survival rate of patients (Fig. 4B–D). Thus, we can consider this risk score as a tool for predicting the survival of patients with AML.

3.5. Functional enrichment analysis of PANoptosis-related differentially expressed genes

To further explore the PANoptosis risk signature, we screened genes with differential expression between the high- and low-risk groups and identified 327 PANoptosis-related differentially expressed genes (PRDEGs) (Fig. 5A and B). The expression levels of 309 PRDEGs decreased, and the 327 PRDEGs increased in the high-risk group. These genes were subjected to GO and KEGG analyses. GO analysis revealed a direct correlation between the high-risk score, cytokine-mediated signaling pathway, and cytokine production, implying that the high-risk score was related to cell immunity (Fig. 5C). Similarly, the KEGG analysis indicated that the high-risk score was related to the chemokine signaling pathway, cytokine-cytokine receptor interactions, and B-cell receptor interactions (Fig. 5D). The low-risk score was related to extracellular composition and structure, collagen metabolic processes, and neutrophil-mediated killing (Fig. 5E and F). To further reveal the correlation between the risk score and cell immunity, we performed GSEA, which evaluated the pathways more comprehensively. Consistent with the above results, GSEA revealed that immune-related biological processes were more significant in the high-risk group (Fig. 5G and H). Therefore, we hypothesized that the risk score is relevant to the immune features of AML cells.

3.6. Immune cells infiltration analysis in the high- and low-risk groups

We evaluated immune cell infiltration characteristics in the AML tumor microenvironment based on risk scores. The results of the xCell algorithm revealed an obvious difference between the high- and low-risk groups (Fig. 6A). More immune cells, such as $CD4^+$ naive T-cells, macrophages, and monocytes, were found in high-risk AML patients. CMP and MSC showed greater infiltration in the low-risk group. We also investigated the correlation between immune cell infiltration and risk score using ssGSEA. The results also showed that more immune cells were present in the high-risk group (Fig. 6B and C). Similarly, the expression levels of many model factors were associated with immune cell infiltration (Fig. 6D). Among the model factors, BIRC3 and PELI1 were positively correlated with $CD4^+$ T cells, $CD8^+$ T cells, B cells, natural killer cells, dendritic cells, neutrophils, macrophages, regulatory T cells, and T helper cells. ELANE and IL1R1 expression levels were negatively correlated with T helper cells, $CD8^+$ T cells, dendritic cells, and monocytes. The TIMER, EPIC, and MCPcounter algorithms correlate similarly (Fig. S1). In addition, we evaluated the tumor-immune microenvironment in the GSE37642 cohort, and the results were similar to those in the TCGA cohort (Fig. S2). Generally, the high-risk group exhibited increased immune cell infiltration. Thus, we predicted that patients with a high-risk score may have a hot tumor-immune microenvironment.

3.7. Correlation between the PANoptosis-risk signature and immunotherapy efficacy

As a new treatment method, immunotherapy is increasingly important. The above analyses proved that the high-risk group may have better immunotherapy potential, which prompted us to further investigate the correlation between risk score and immunotherapy efficacy. We discovered that the risk score was positively correlated with the ESTIMATE, immune, and stromal scores (Fig. 7A). Among the model factors, the expression levels of PELI1, BIRC3, NFKBIA, CASP10, and PRKACG were positively correlated with the immune score, whereas that of ELANE was negatively correlated (Fig. 7B). Next, the expression levels of immune checkpoints (ICs) were compared between the two risk groups. We believe there were higher expression levels of ICs in the high-risk group, especially of PD-1, PD-L1, and PD-L2 (Fig. 7C). We further explored the model factors associated with the expression of ICs (Fig. 7D). When BIRC3, PELI1, CASP10, PRKACG, NFKBIA, AKT1, and TREM2 were highly expressed, IC expression levels were also high. When ELANE was highly expressed, the expression of ICs were low. These findings indicated that many model factors have the potential to be used as predictors and targets for immunotherapy. Therefore, we comprehensively evaluated these model factors by calculating their TIDE scores (Fig. 7E). Three model factors were identified as predictors of immunotherapeutic efficacy: BIRC3, PELI1, and PRKACG.

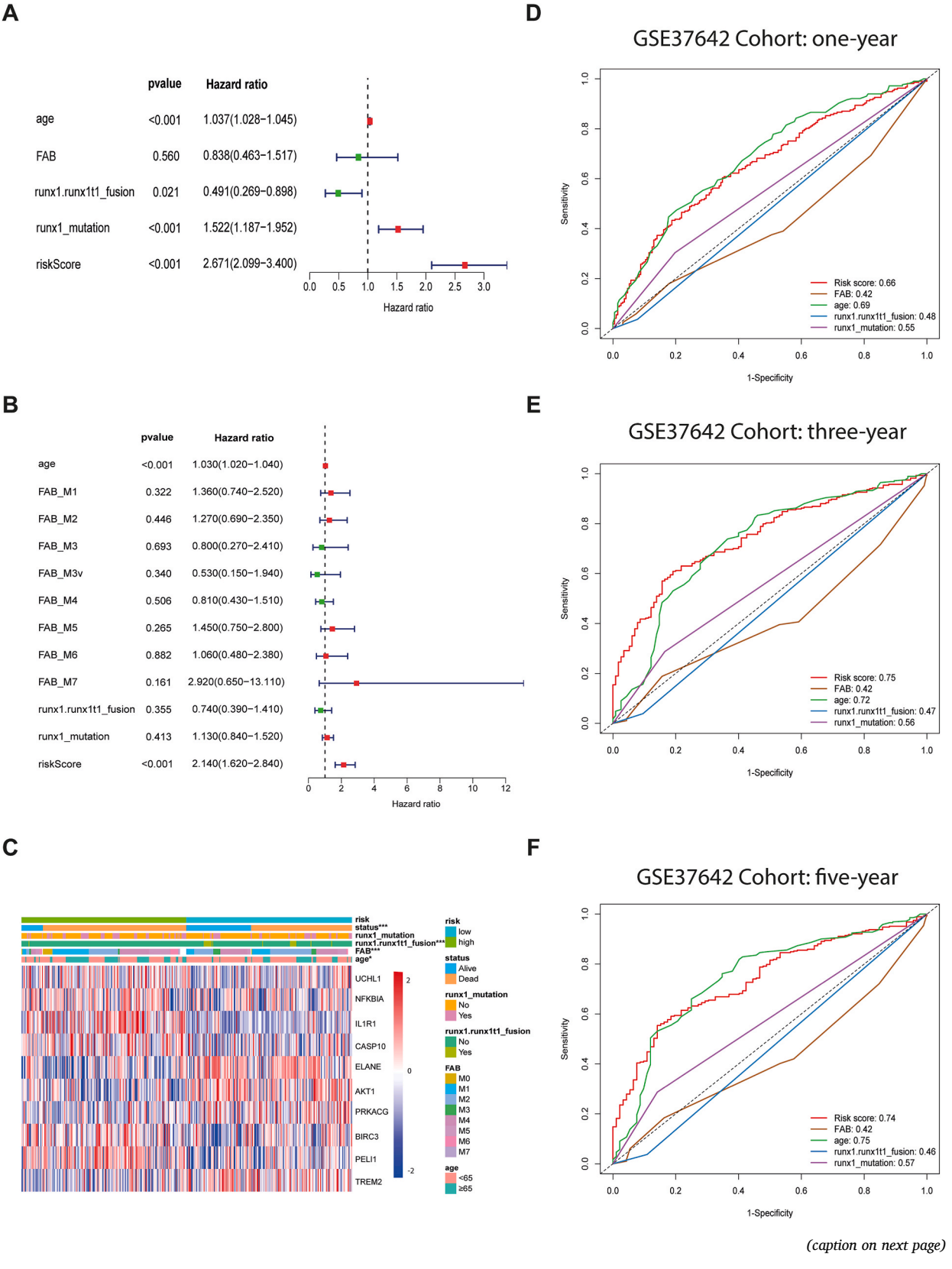

(caption on next page)

Fig. 3. Comparison between clinicopathological characteristics and PANoptosis-risk signature. (A–B) Univariate and multivariate Cox regression analysis of clinicopathological characteristics and risk score by GSE37642 cohort. (C) The relationship of clinicopathological characteristics and PANoptosis-risk signature expression levels. (D–F) Time-dependent ROC curve of clinicopathological characteristics and risk score for predicting 1-,3- and 5-year overall survival by GSE37642 cohort.

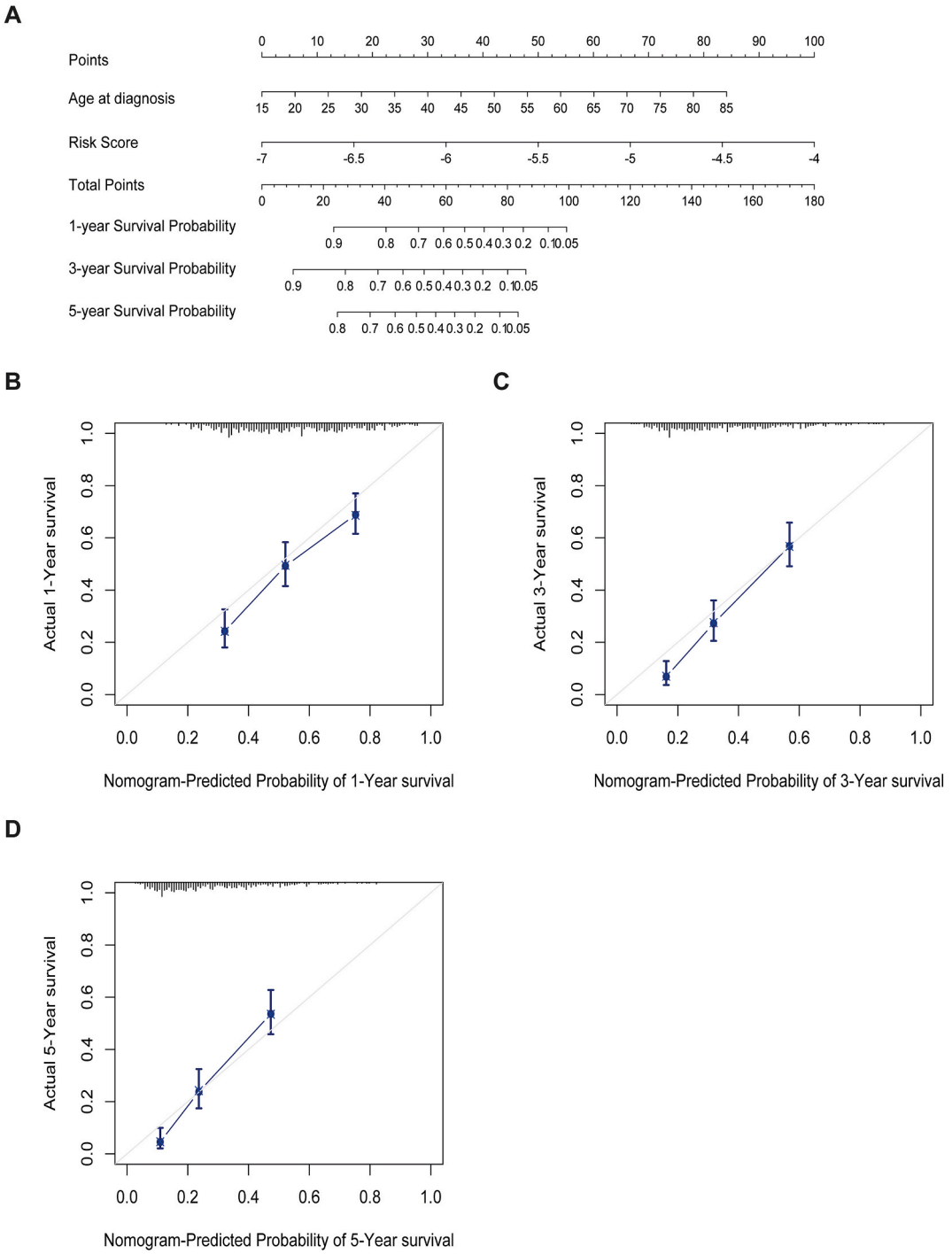

Fig. 4. Establishment of the Nomogram. (A) Nomogram was established to predict 1-, 3-, 5-year survival rates of AML patients in GSE37642 cohort. (B–D) Calibration curves showed the concordances between predicted and observed 1-, 3-, 5-year survival rates of AML patients based on the nomogram in GSE37642 cohort.

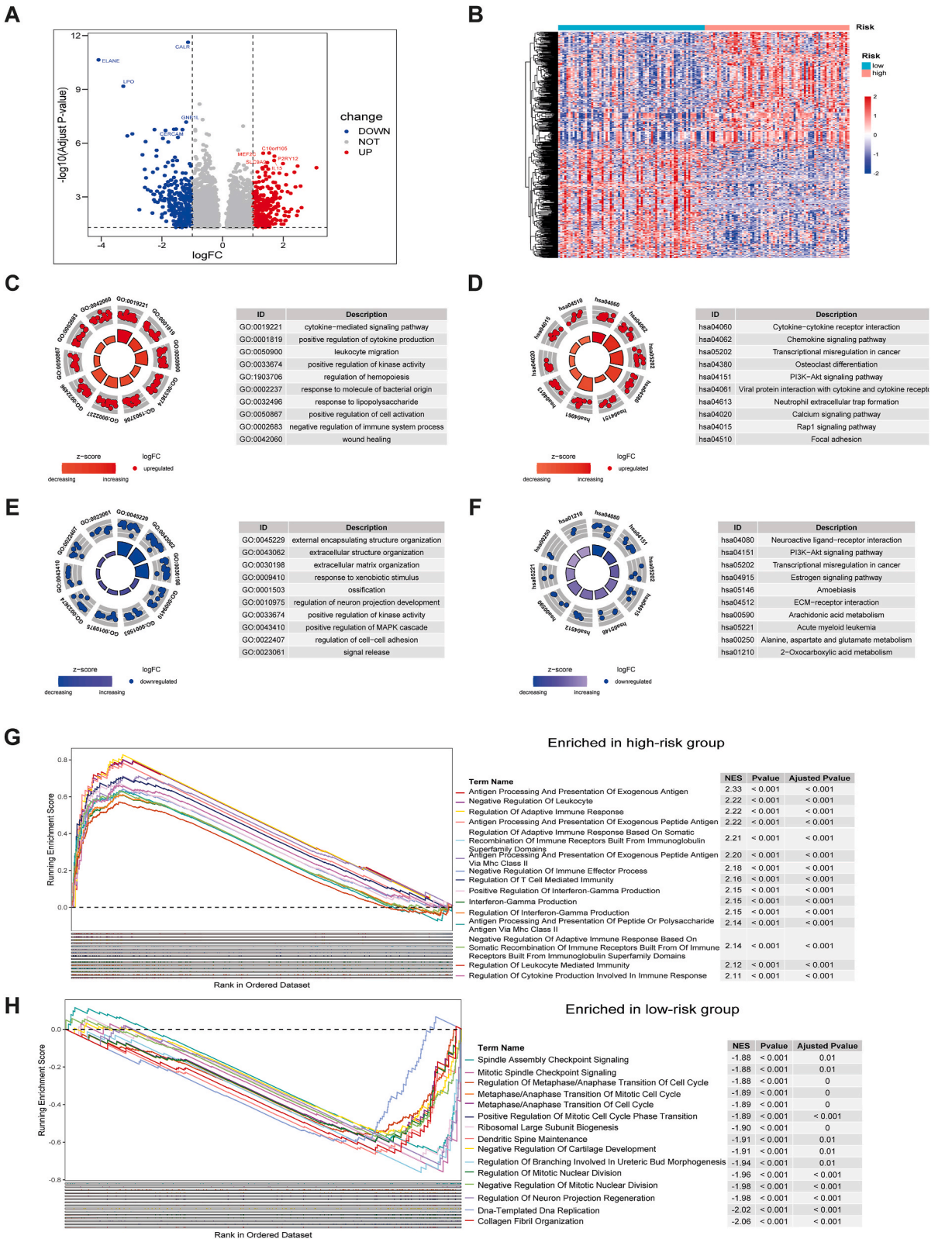

ID	Description
GO:0019221	cytokine−mediated signaling pathway
GO:0001819	positive regulation of cytokine production
GO:0050900	leukocyte migration
GO:0033674	positive regulation of kinase activity
GO:1903706	regulation of hemopoiesis
GO:0002237	response to molecule of bacterial origin
GO:0032496	response to lipopolysaccharide
GO:0050867	positive regulation of cell activation
GO:0002683	negative regulation of immune system process
GO:0042060	wound healing

ID	Description
hsa04060	Cytokine−cytokine receptor interaction
hsa04062	Chemokine signaling pathway
hsa05202	Transcriptional misregulation in cancer
hsa04380	Osteoclast differentiation
hsa04151	PI3K−Akt signaling pathway
hsa04061	Viral protein interaction with cytokine and cytokine recept
hsa04613	Neutrophil extracellular trap formation
hsa04020	Calcium signaling pathway
hsa04015	Rap1 signaling pathway
hsa04510	Focal adhesion

ID	Description
GO:0045229	external encapsulating structure organization
GO:0043062	extracellular structure organization
GO:0030198	extracellular matrix organization
GO:0009410	response to xenobiotic stimulus
GO:0001503	ossification
GO:0010975	regulation of neuron projection development
GO:0033674	positive regulation of kinase activity
GO:0043410	positive regulation of MAPK cascade
GO:0022407	regulation of cell−cell adhesion
GO:0023061	signal release

ID	Description
hsa04080	Neuroactive ligand−receptor interaction
hsa04151	PI3K−Akt signaling pathway
hsa05202	Transcriptional misregulation in cancer
hsa04915	Estrogen signaling pathway
hsa05146	Amoebiasis
hsa04512	ECM−receptor interaction
hsa00590	Arachidonic acid metabolism
hsa05221	Acute myeloid leukemia
hsa00250	Alanine, aspartate and glutamate metabolism
hsa01210	2−Oxocarboxylic acid metabolism

Term Name	NES	Pvalue	Ajusted Pvalue
Antigen Processing And Presentation Of Exogenous Antigen	2.33	< 0.001	< 0.001
Negative Regulation Of Leukocyte	2.22	< 0.001	< 0.001
Regulation Of Adaptive Immune Response	2.22	< 0.001	< 0.001
Antigen Processing And Presentation Of Exogenous Peptide Antigen	2.22	< 0.001	< 0.001
Regulation Of Adaptive Immune Response Based On Somatic Recombination Of Immune Receptors Built From Immunoglobulin Superfamily Domains	2.21	< 0.001	< 0.001
Antigen Processing And Presentation Of Exogenous Peptide Antigen Via Mhc Class II	2.20	< 0.001	< 0.001
Negative Regulation Of Immune Effector Process	2.18	< 0.001	< 0.001
Regulation Of T Cell Mediated Immunity	2.16	< 0.001	< 0.001
Positive Regulation Of Interferon-Gamma Production	2.15	< 0.001	< 0.001
Interferon-Gamma Production	2.15	< 0.001	< 0.001
Regulation Of Interferon-Gamma Production	2.15	< 0.001	< 0.001
Antigen Processing And Presentation Of Peptide Or Polysaccharide Antigen Via Mhc Class II	2.14	< 0.001	< 0.001
Negative Regulation Of Adaptive Immune Response Based On Somatic Recombination Of Immune Receptors Built From Of Immune Receptors Built From Immunoglobulin Superfamily Domains	2.14	< 0.001	< 0.001
Regulation Of Leukocyte Mediated Immunity	2.12	< 0.001	< 0.001
Regulation Of Cytokine Production Involved In Immune Response	2.11	< 0.001	< 0.001

Term Name	NES	Pvalue	Ajusted Pvalue
Spindle Assembly Checkpoint Signaling	-1.88	< 0.001	0.01
Mitotic Spindle Checkpoint Signaling	-1.88	< 0.001	0.01
Regulation Of Metaphase/Anaphase Transition Of Cell Cycle	-1.88	< 0.001	0
Metaphase/Anaphase Transition Of Mitotic Cell Cycle	-1.89	< 0.001	0
Metaphase/Anaphase Transition Of Cell Cycle	-1.89	< 0.001	0
Positive Regulation Of Mitotic Cell Cycle Phase Transition	-1.89	< 0.001	< 0.001
Ribosomal Large Subunit Biogenesis	-1.90	< 0.001	0
Dendritic Spine Maintenance	-1.91	< 0.001	0.01
Negative Regulation Of Cartilage Development	-1.91	< 0.001	0.01
Regulation Of Branching Involved In Ureteric Bud Morphogenesis	-1.94	< 0.001	0.01
Regulation Of Mitotic Nuclear Division	-1.96	< 0.001	< 0.001
Negative Regulation Of Mitotic Nuclear Division	-1.98	< 0.001	< 0.001
Regulation Of Neuron Projection Regeneration	-1.98	< 0.001	< 0.001
Dna-Templated Dna Replication	-2.02	< 0.001	< 0.001
Collagen Fibril Organization	-2.06	< 0.001	< 0.001

Fig. 5. Functional enrichment analysis of PANoptosis-related differentially expressed genes (PRDEGs) by TCGA cohort. (A–B) The volcano and heatmaps of PRDEGs between the high and low-risk group. (C–D) GO and KEGG analysis of PRDEGs in the high-risk group. (E–F) GO and KEGG analysis of PRDEGs in the low-risk group. (G) GSEA analysis of PRDEGs in the high-risk group. (H) GSEA analysis of PRDEGs in the low-risk group.

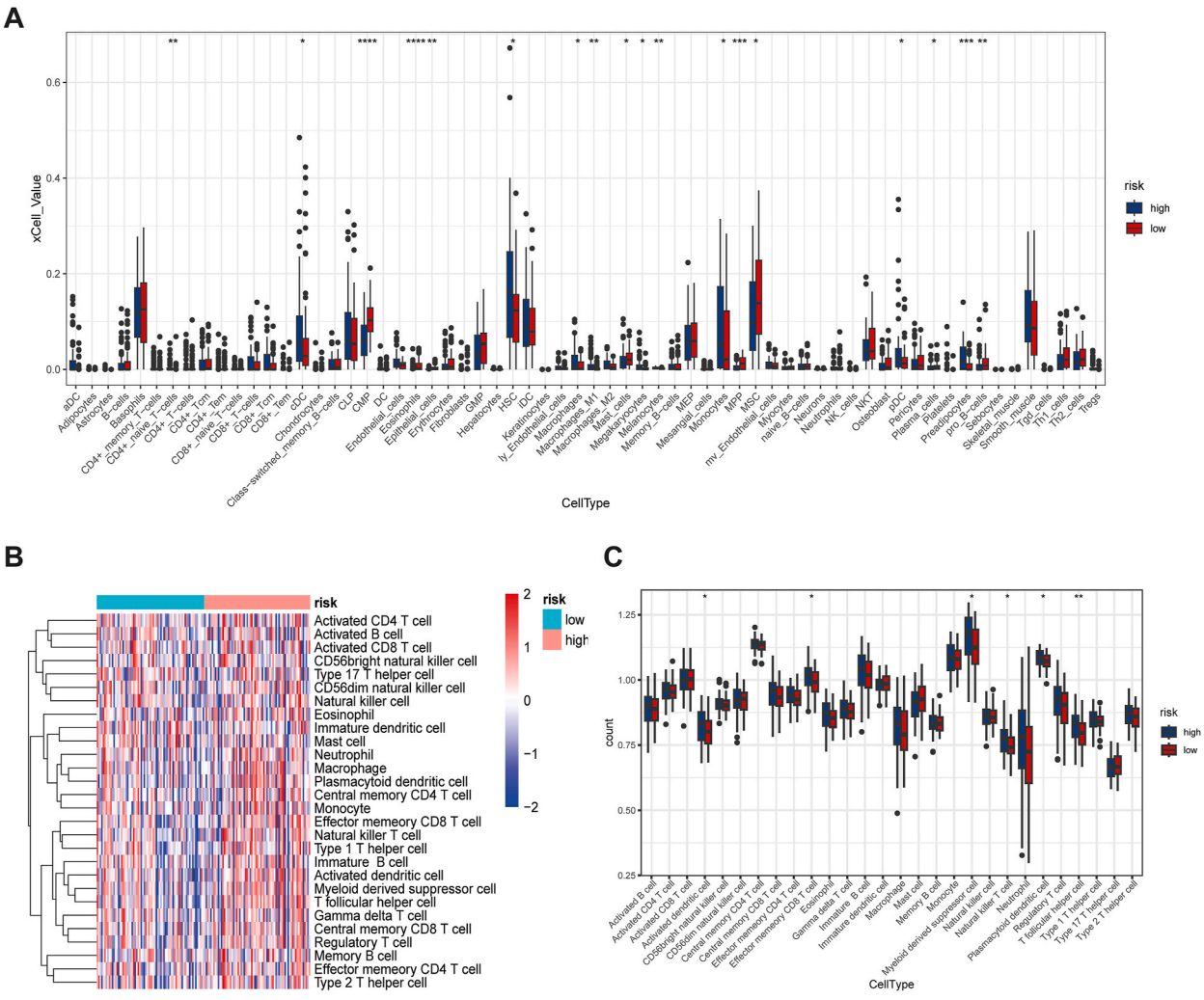

(caption on next page)

Fig. 6. Immune cells infiltration analysis in the high and low-risk groups. (A) The infiltration levels of 64 immune cells in the high and low-risk groups by xCell algorithm in TCGA cohort. (B) The discribution of 28 immune cells in the high and low-risk groups by ssGSEA in TCGA cohort. (C) The infiltration levels of 18 immune cells in the high and low-risk groups by ssGSEA in TCGA cohort. (D) The heatmap of correlation between 10 model genes and 28 immune cells infiltration by ssGSEA in TCGA cohort.

We inferred that high-risk patients with high BIRC3, PELI1, and PRKACG expression possess an activated immune microenvironment and are more likely to benefit from immunotherapy.

3.8. Single-cell sequencing data analysis

To explore the correlation between model factors and the AML tumor microenvironment, we conducted single-cell sequencing analysis using the GSE116256 dataset. The cellular components of the bone marrow samples from AML patients, AML patients after chemotherapy, and healthy individuals were clustered and annotated (Fig. 8A). Fig. 8B–E exhibited the expression levels and distributions of the nine model factors. NFKBIA was widely expressed in bone marrow tissue, with expression levels varying greatly in T cells from the normal group, leukemia progenitor cells from the AML treatment group, and progenitor cells from the AML group (Fig. 8B). ELANE was upregulated in relatively primitive cells, such as leukemia progenitor cells in the AML group and granulocyte-macrophage progenitor (GMP) cells (Fig. 8C). Additionally, the expression of BIRC3 and PELI1 was enriched in plasma and B cells, and BIRC3 expression was notably elevated in T cells (Fig. 8D). Based on the specific expression mentioned above, we speculated that NFKBIA and ELANE might play a role in the onset and late drug resistance of AML, whereas BIRC3 and PELI1 may participate in early drug resistance of AML by regulating the bone marrow microenvironment. The results of the GO analysis partially supported this concept (Fig. 8F). NFKBIA regulates hematopoiesis and differentiation of myeloid cells in the bone marrow and is involved in the regulation of the immune system. The enrichment results of ELANE were different from the expression results, indicating its involvement in the human inflammatory response and humoral immunity; however, this was not clearly demonstrated in the expression analysis. We found that PELI1 was widely involved in the process of human immune regulation to promote the proliferation of B cells and inhibit the proliferation of lymphocytes and T cells and that BIRC3 was more significantly involved in the immune response to viral infections. Thus, we inferred that PELI1 and BIRC3 may participate in the regulation of the immune microenvironment in patients with AML. Therefore, special attention should be given to NFKIBA with regard to the occurrence of AML.

3.9. Screening susceptible drugs

Chemotherapy remains the primary treatment option for AML. However, drug resistance and the severe adverse effects of chemotherapy pose obstacles for AML patients. Therefore, identifying novel treatment regimens for AML is important. The boxplot in Fig. S3 shows the differential expression levels of the 10 PRGs in the GSE37642 cohort. We found that CASP10, PELI1, UCHL1, NFKBIA, BIRC3, and IL1R1 expression levels were associated with high-risk scores, whereas AKT1, ELANE, TREM2, and PRKACG expression levels were highly correlated with low-risk scores. Based on the above results, BIRC3, PELI1, and PRKACG performed better at predicting the efficacy of immunotherapy. By combining the expression data, we confirmed that BIRC3 and PELI1 are risk factors for AML. Therefore, we performed a drug sensitivity analysis for these two genes. Camptothecin, dactinomycin, AZD-8186, and BDP-9066 were sensitive drugs targeting BIRC3 (Fig. S4A). BDP-9066, ipatasertib, GNE-317, NVP-ADW742, AZD5363, camptothecin, pictilisib, Wnt-C59, dactolisib, docetaxel-1007, paclitaxel, and AZD8186 were all sensitive to PELI1 (Fig. S4B).

Based on the correlation coefficient, we selected the top four drugs for molecular docking to further validate the correlation between the drugs and proteins, and the 3D structures of the target proteins and drugs were downloaded (Fig. 9A–B, Fig. 10A and B, and Fig. S5A). Molecular docking was performed to determine the binding mode between the proteins and drugs (Table S2). For BIRC3, camptothecin, AZD-8186, and BDP-9066 exhibited strong binding capacities (Fig. 9C–K). BDP-9066, GNE-317, ipatasertib, and NVP. ADW742 demonstrated a robust binding affinity for PELI1 (Fig. 10C–K and Figs. S5B–D). The binding sites for camptothecin, AZD-8186, and BDP-9066 on BIRC3 are slightly different, with binding energies of −8.14 kcal/mol, −7.12 kcal/mol, and −5.96 kcal/mol, respectively (Table S2). Camptothecin formed hydrogen bonds with amino acids Asp296 (A), Arg244 (B), and Thr246 (B) (Fig. 9D and E). AZD-8186 also showed excellent docking results, forming hydrogen bonds directly with Asn249 and Arg324 of BIRC3 (Fig. 9G and H). The docking results for BDP-9066 were slightly inferior to those for camptothecin and AZD-8186, as it could only bind directly to Asp296 (Fig. 9J and K). There were also many stable H-bond structures between the drugs and PELI proteins, such as BDP-9066 and Thr117 and Pro385 amino acids (Fig. 10D and E), GNE-317 and Asn26 amino acids (Fig. 10G and H), ipatasertib and Ala13, Pro14, Glu257 (Fig. 10J and K), and NVP.ADW742 and Glu171 (Figs. S5C and D).

3.10. Molecular dynamics simulation

The above docking results showed that these small compounds could indeed target and bind to BIRC3 and PELI1 proteins. Subsequently, we assessed binding stability using molecular dynamics simulations (MDS). First, the root mean square deviation (RMSD) of ligands and proteins in molecular dynamics trajectories was used to measure the changes in ligand and protein structures over time from the initial moment (Fig. 11A–F). With the exception of BDP-9066 (with the BIRC3 protein) and ipatasertib (Fig. 11C and F), the RMSD values for all other compounds were less than 5 Å when they reached a stable state (Fig. 11A, B, D, and E), indicating that their conformations underwent minimal changes compared to their initial states. Camptothecin, AZD-8186, BDP-9066 (with the PELI1

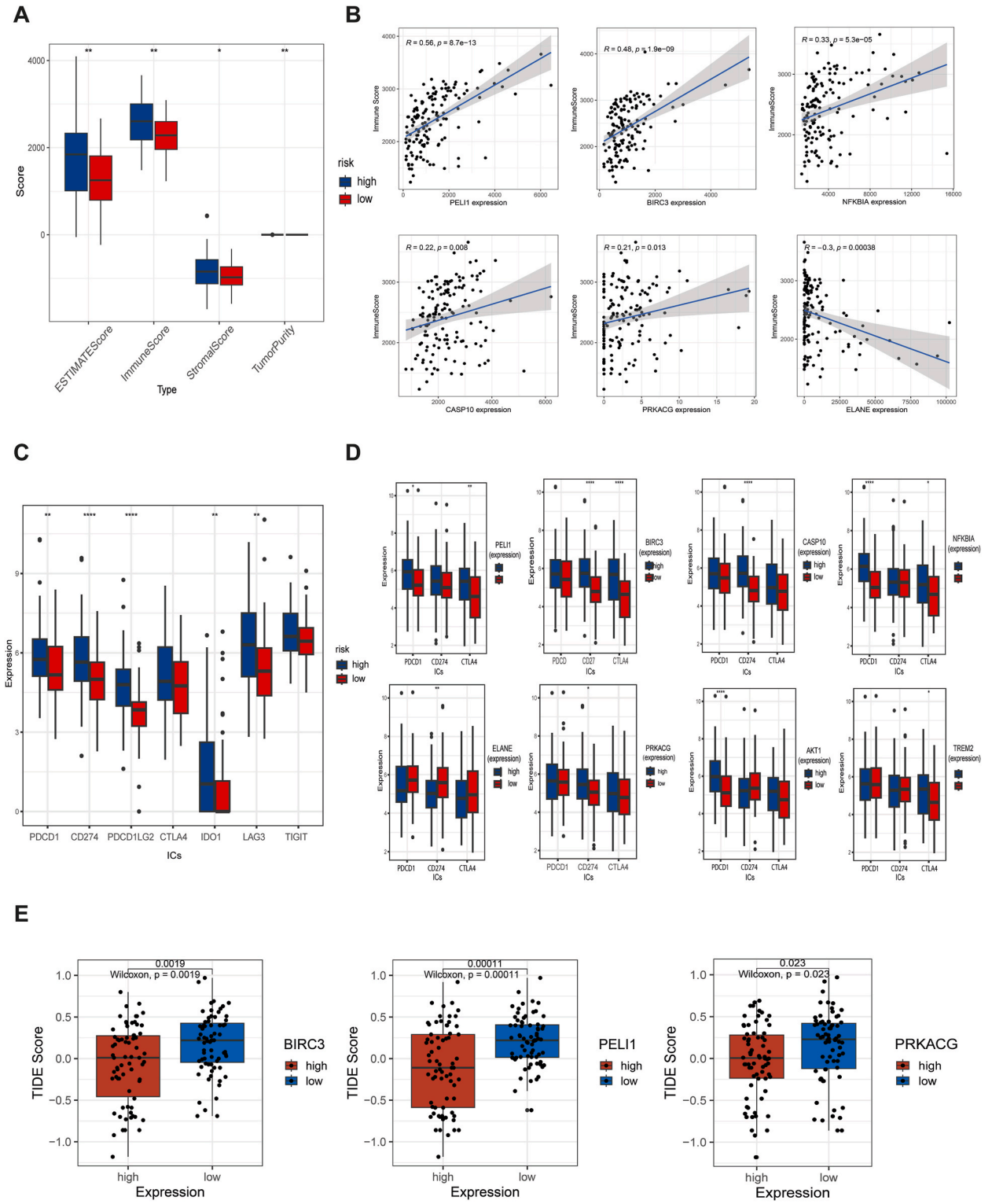

Fig. 7. Correlation between the PANoptosis-risk signature and immunotherapy efficacy by TCGA cohort. (A) The box chart of immune score in the high and low-risk group. (B) Scatter diagrams of correlation between immune score and model factors expression. (C) The box chart of immune checkpoints expression in the high and low-risk group. (D) The box chart of immune checkpoints expression with different expressed model factors. (E) The box chart of TIDE score with different expressed model factors.

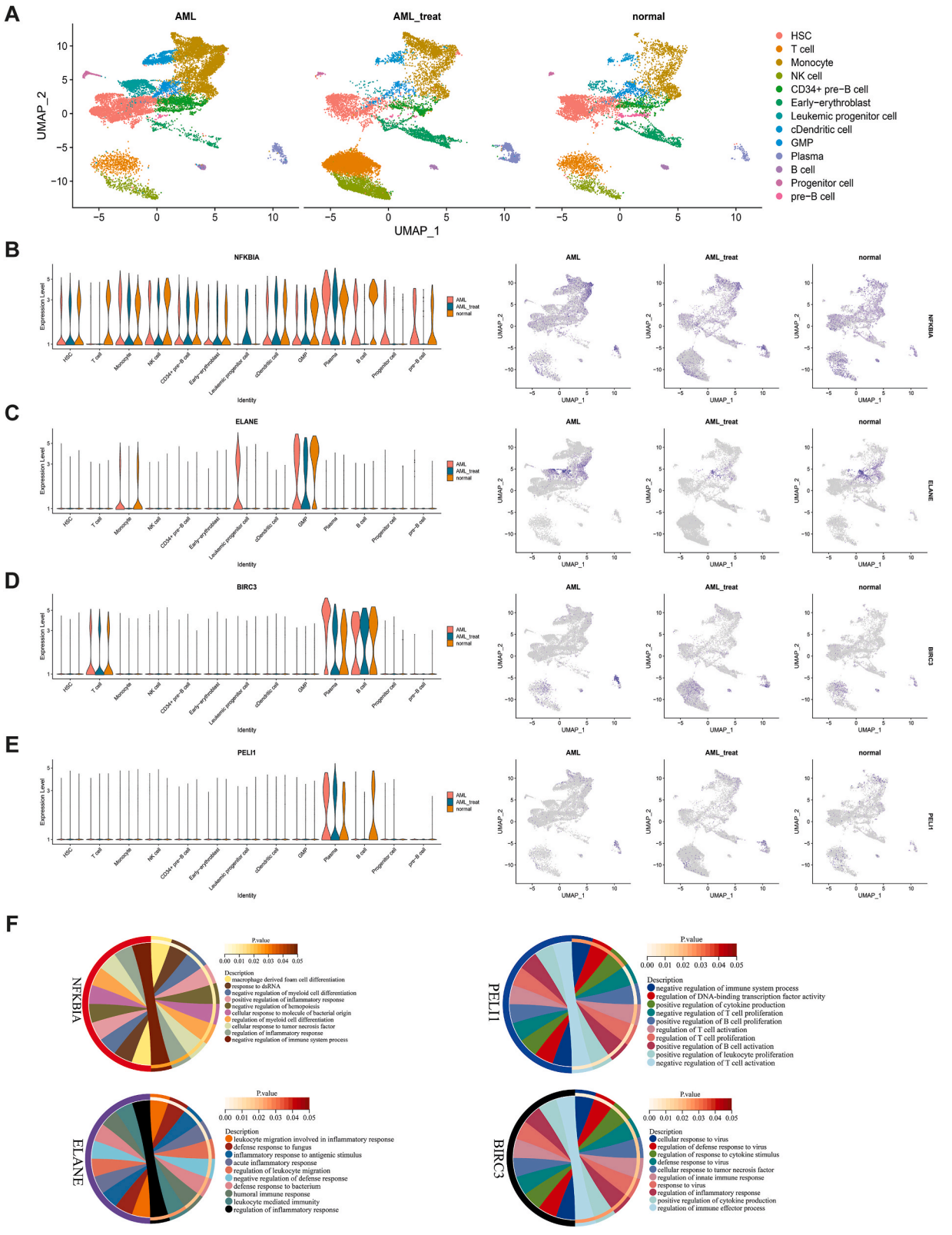

Fig. 8. Model factors analysis based on the single-cell sequencing data using AML GSE116256 **cohort.** (A) Cell clusters of bone marrow samples from three groups of patients in GSE116256. (B–E) Expression levels and distributions of model genes in different cells of different groups. (B) NFKBIA, (C) ELANE, (D) BIRC3, (E) PELI1. (F) Chord diagram of immune-related pathway of four sensitive factors.

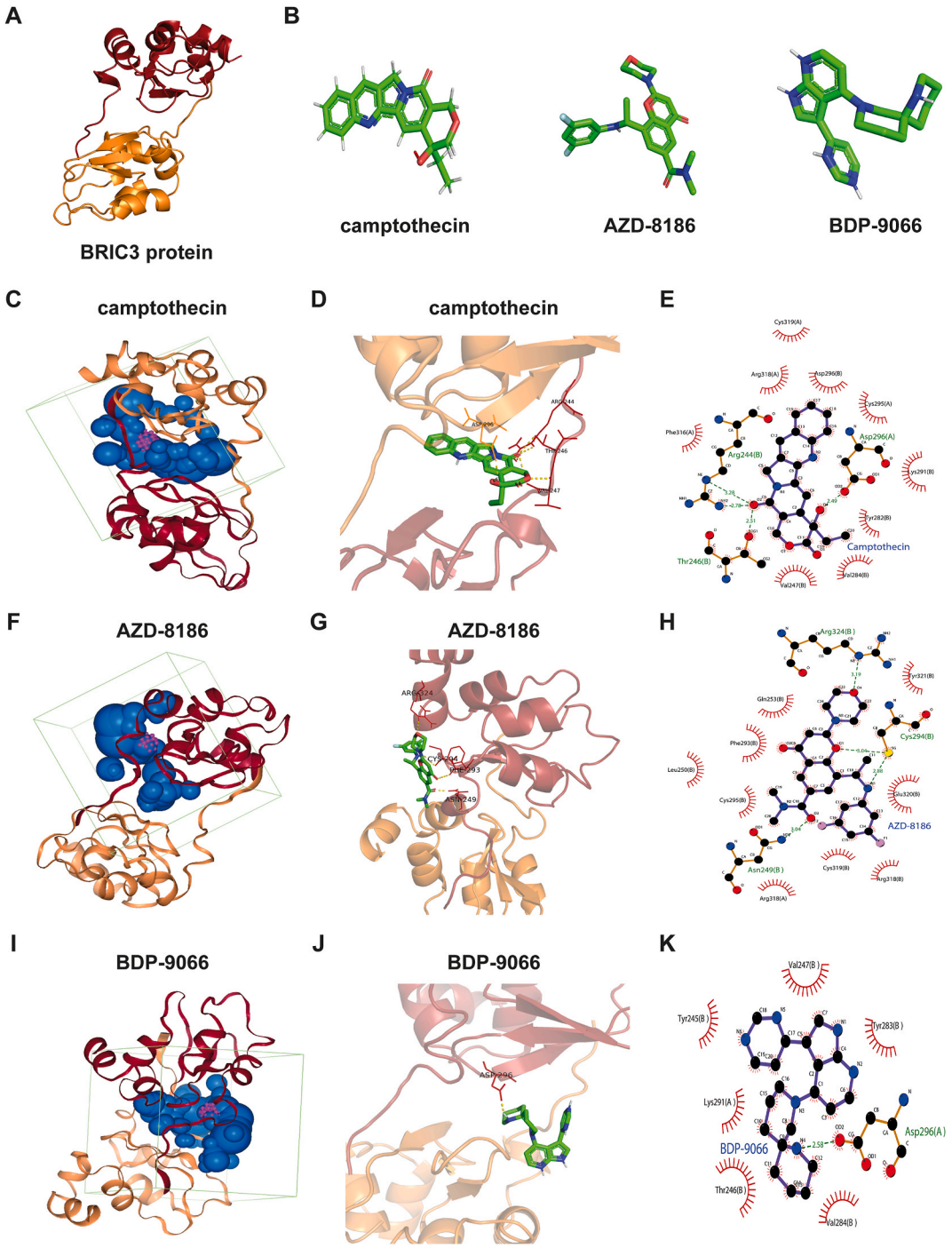

Fig. 9. Molecular docking for BIRC3 protein and sensitive drugs. (A) 3D structure of BIRC3 protein. (B) 3D structure of drugs: camptothecin, AZD-8186, BDP-9066. (C) The binding site and box of camptothecin on BIRC3 protein. (D) The optimal docking space conformation of the camptothecin to BIRC3 protein. (E) The interaction force between BIRC3 protein and camptothecin. (F–H) AZD-8186. (I–K) BDP-9066.

protein), and GNE-317 demonstrated stable binding to target proteins.

From the surface to the point, we further validated the changes in each residue of the target protein by root mean square fluctuation (RMSF) during the binding process. The average RMSF values for camptothecin, AZD-8186, BDP-9066 (with PELI1 protein), and GNE-317 were low (Fig. 11G, H, J, and K), indicating that these drugs effectively reduced fluctuations in the amino acid residues of the protein. This finding demonstrates that these drugs interact strongly with proteins. In contrast, BDP-9066 (with the BIRC3 protein) failed to stably bind to the protein, resulting in significant fluctuations across all amino acid residues (Fig. 11I). Additionally,

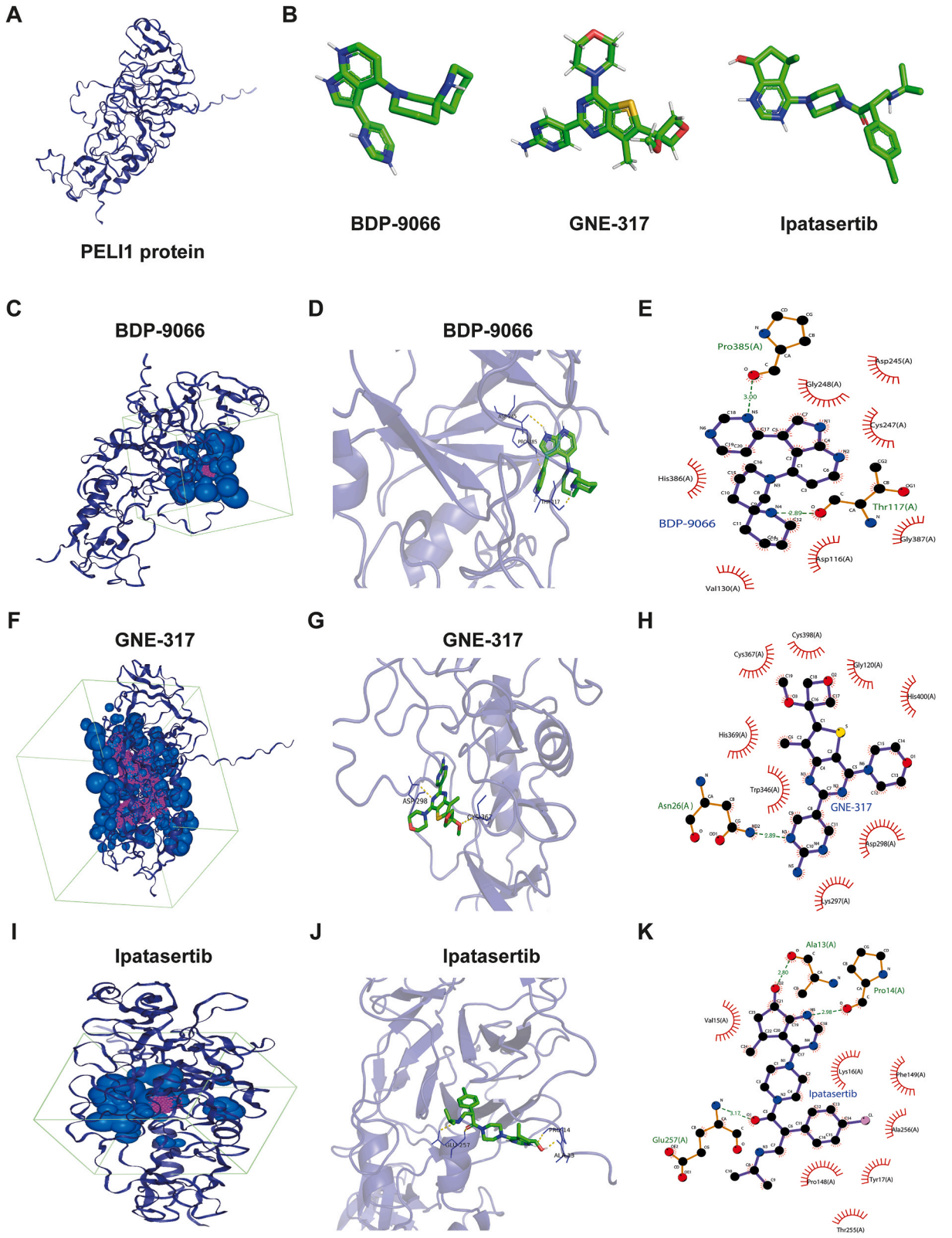

Fig. 10. Molecular docking for PELI1 protein and sensitive drugs. (A) 3D structure of PELI1 protein. (B) 3D structure of drugs: BDP-9066, GNE-317, Ipatasertib. (C) The binding sites and box of BDP-9066 on PELI1 protein. (D) The optimal docking space conformation of the BDP-9066 to PELI1 protein. (E) The intera force between PELI1 protein and BDP-9066. (F–H) GNE-317. (I–K) Ipatasertib.

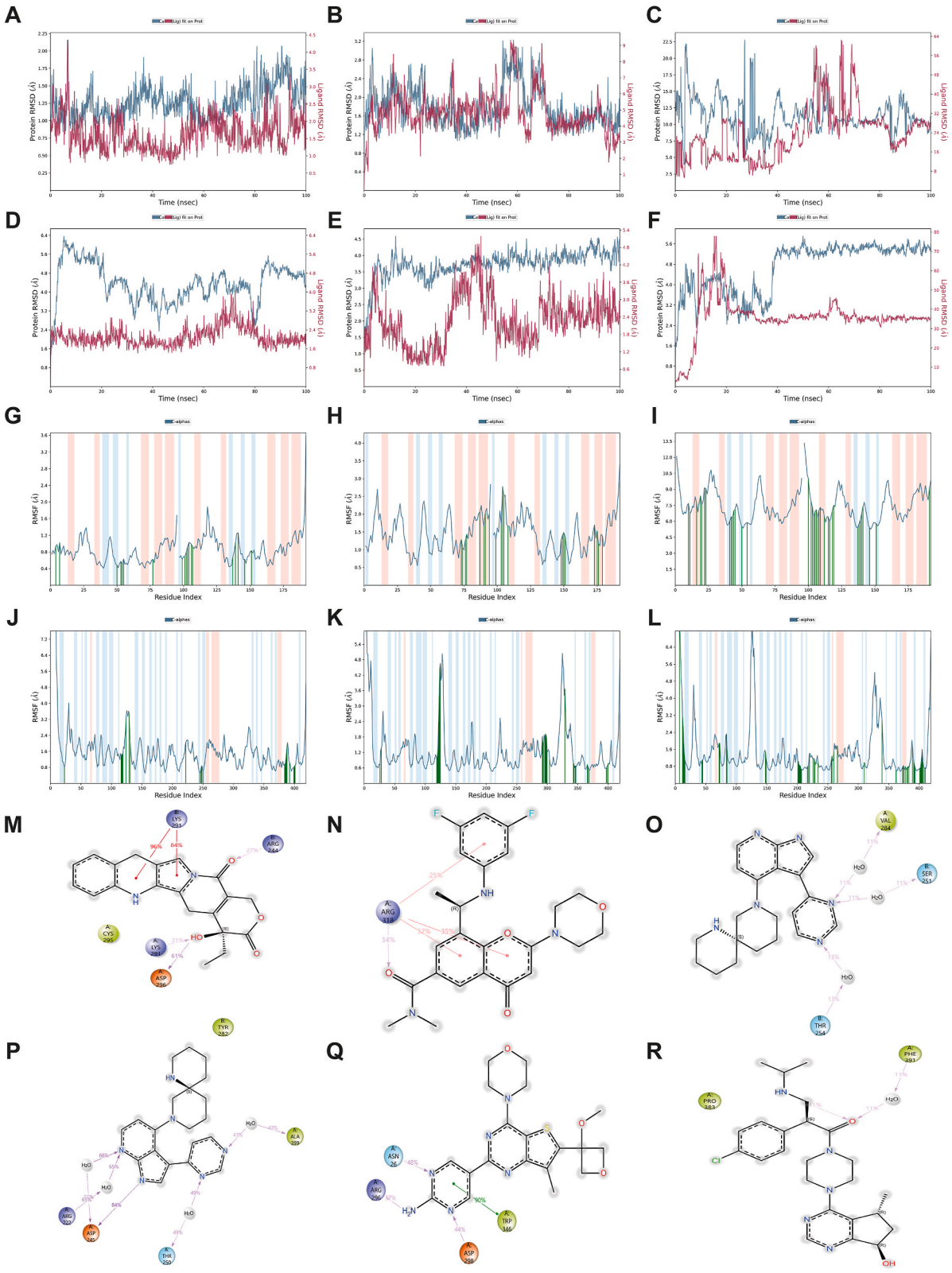

Fig. 11. Molecular dynamics simulation between BIRC3/PELI1 proteins and six drugs. (A–F) Line chart of RMSD in 100ns simulations. Camptothecin, AZD-8186, BDP-9066 (with BIRC3 protein), BDP-9066 (with PELI1 protein), GNE-317, and ipatasertib. (G–L) Line chart of RMSF in 100ns simulations. (M–R) Detailed interaction diagram of drugs atoms and proteins residues.

ipatasertib exhibited considerable conformational changes, leading to unstable binding to the target protein and resulting in high RMSF values in some scenarios (Fig. 11L). Among the drugs tested, camptothecin and BDP-9066 (with PELI1) displayed the strongest specific binding to proteins and significantly reduced amino acid fluctuations (Fig. 11G and J).

Finally, we presented a detailed plot of the interaction between drug atoms and protein residues and screened for interactions that occurred in trajectories (0.00–100.00 ns) with simulation times exceeding 10.0 %. Camptothecin, AZD-8186, BDP-9066 (with PELI1 protein), and GNE-317 showed multiple interactions with amino acid residues, and the interaction times were relatively long (Fig. 11M, N, P, and Q). The interaction time between BDP-9066 (with BIRC3 protein), ipatasertib, and amino acid residues was approximately 10 %, which was why they could not stably bind to the proteins (Fig. 11O and R). Through further calculations of binding stability, we concluded that camptothecin, AZD-8186, BDP-9066 (with the PELI1 protein), and GNE-317 could form relatively stable binding sites with the target proteins, thereby enhancing the stability of the protein structure and reducing fluctuations in amino acid residues.

4. Discussion

It is well known that AML cells are immortal. The high recurrence rate and drug resistance of AML are attributed to disordered cell death pathways, such as apoptosis, pyroptosis, and necroptosis. A recent study discovered a new cell death pattern called PANoptosis, which is an inflammatory cell death pathway. PANoptosis combines the main proteins and biological programs of apoptosis, pyroptosis, and necroptosis [6,17,18]. The molecular basis, mechanism of action, and biological functions of PANoptosis have been explored in many tumor types [27]. For example, the broad-spectrum anticancer drug sulconazole can stimulate mitochondrial oxidative stress and suppress glycolysis to induce PANoptosis, which enhances the radiosensitivity of esophageal cancer [28]. IRF1 could prevent tumorigenesis by regulating PANoptosis in colorectal cancer [29]. As a promising direction, the research on PANoptosis in AML was still superficial. Pan-cancer research on PANoptosis by Zhuang et al. showed that AML had the highest PANoptosis score and was associated with the tumor microenvironment in various cancers [30]. However, the subsequent analysis was insufficient and did not further explore the key genes that cause disease or drug resistance and indicators with clinical application prospects, providing only a broad and clear direction for subsequent research. Hence, our study screened PANoptosis-related genes using the transcriptome data of AML patients to perform biomarker-based risk stratification for prognostic analysis. Univariate, multivariate, and LASSO Cox regression analyses were performed, and 10 model factors were screened to establish the PANoptosis-risk signature. We found that high-risk group patients were prone to have a shorter survival time. Therefore, the PANoptosis risk signature can be considered as a prognostic biomarker for AML. Similarly, Zhang et al. established a PANoptosis-related prognostic model for pancreatic cancer [31]. Song et al. reported an association between PANoptosis and the prognosis of gliomas [32]. In hepatocellular carcinoma, the PANoptosis-based model was identified as a potential biomarker for predicting survival [33]. Therefore, the application of the PANoptosis risk signature for prognostic analysis may be useful in future clinical studies.

There are limited drugs available to patients due to drug resistance to chemotherapy. And the severe adverse effects make patients painful and decrease the body resistance. Therefore, targeted therapy, particularly immunotherapy, is the superior choice. Immune cells and immune factors widely exist in the blood and bone marrow; therefore, they are easier for patients with AML to mobilize to achieve therapeutic goals. Currently, studies on immunotherapy for AML have made great progress, especially CAR-T. Due to the high cost and specific side effects, such as cytokine release syndrome, more accurate biomarkers need to be explored for the prediction of immunotherapy efficacy. Recent studies have revealed the importance of PANoptosis in predicting the immunotherapeutic response in prostate adenocarcinoma, hepatocellular carcinoma, and gastric cancer [27,34,35]. Our study focused on PANoptosis and revealed its correlation with the immune features of AML. We also discovered that a high-risk score was related to cell immunity, including immune cell infiltration, immune scores, and immune checkpoint gene expression. Similar conclusions have been reached by Tang et al.; however, in their study, only immune analyses were performed, and the results were not verified. Their study was limited to signatures and lacked research on sensitive genes [36]. Our results complement those of Tang et al. We performed an immune analysis and verified this at the cellular level using the GSE116256 cohort. Sensitive genes, such as BIRC3, PELI1, and targeted drugs, were screened. Subsequently, molecular docking and molecular dynamics simulations were performed to confirm the reliability of the drug. Therefore, our study provides more accurate genes and drugs for the clinical classification and combined drug resistance screening of patients with AML. Among the sensitive genes, BIRC3 was significantly positively correlated with the above cellular immune features. This indicated that AML patients with high BIRC3 expression have a hot immune microenvironment. Indeed, the TIDE score indicated that patients with high BIRC3 expression may respond better to immunotherapy. The role of BIRC3 in the immune microenvironment was assessed by constructing different signatures. In line with this, immune-related genes, including BIRC3, were positively correlated with immunomodulatory subtypes in triple-negative breast cancer [37]. However, in lung adenocarcinoma, necroptosis-related genes, including BIRC3, are associated with immunotherapy tolerance [38]. BIRC3 has been considered as an inhibitor of PANoptosis [39] and is positively correlated with tumor progression, metastasis, recurrence, and chemoresistance [40]. BIRC3 shows the same manifestations as AML [41]. Similarly, the present study revealed that BIRC3 is a risk factor for AML. Given the role of BIRC3 in AML, we hypothesized that BIRC3 may be a new target for immunotherapy. Therefore, we screened a series of sensitive drugs targeting BIRC3 using bioinformatic predictions and virtual screening. We hypothesized that targeting BIRC3 alone or in combination with immune checkpoint inhibitors could improve outcomes. Another gene that significantly positively correlated with the immune microenvironment was PELI1. PELI1 controls necroptosis through the ubiquitination of RIPK1 to activate RIPK3 and MLKL, resulting in the formation of the RIPK1-RIPK3 necrosome [42]. Caspase-1 and IL-1β are crucial factors in cell death and inflammatory reactions. PELI1 regulates inflammatory responses by mediating the NLRP3 inflammasome and ASC to promote caspase-1 activation and IL-1β maturation [43]. This theory may account for the fact that the high expression of PELI1 is associated with a hot immune

microenvironment in AML. Similar to BIRC3, PELI1 may be a predictor of immunotherapy efficacy. PELI1 promotes the development and metastasis of many tumors and is associated with poor prognosis. To the best of our knowledge, this is the first study to verify that PELI1 is a risk factor for AML. Additionally, our results showed that NFKBIA, TREM2, and PRKACG correlated with a hot immune microenvironment. NFKBIA encodes an inhibitor of NF-κB, which is a well-known inflammatory regulator associated with cancer progression [44,45]. NFKBIA polymorphisms are significantly associated with the risk of various cancers [46]. We also demonstrated that NFKBIA is a risk factor in AML. TREM2 inhibits the NLRP3 inflammasome to protect macrophages from bacterial infection-induced apoptosis. In tumors, TREM2 is expressed in macrophages and is responsible for tumor growth. Targeting TREM2 can enhance the T cell response to PD1 inhibitors [47]. In contrast, TREM2 was positively correlated with gamma delta T cells, regulatory T cells, and monocytes in AML. TREM2 could not predict the immunotherapy response in AML. As a subunit of protein kinase (PKA), PRKACG is involved in RUNX1 mutations in AML patients [48]. Interestingly, our study confirmed that PRKACG is beneficial in selecting patients for immunotherapy.

In contrast, our study showed that ELANE, IL1R1, and UCHL1 correlated with a cold immune microenvironment. Previous studies showed that ELANE cleaves and activates GSDMD to mediate pyroptosis in neutrophils [49]. AML susceptibility is characterized by cyclic neutropenia (CyN) and severe congenital neutropenia (SCN). Heterozygous mutations in ELANE could cause CyN and SCN [54]. Similarly, granulocyte colony-stimulating factor (G-CSF) also induces leukemia cell pyroptosis by targeting ELANE [50]. ELANE is of great value for the treatment of refractory and recurrent AML. This study showed that ELANE is associated with a cold immune microenvironment. Hence, we speculated that ELANE results in a cold tumor state, and targeting ELANE could reverse this phenomenon. There are many complex biological actions of the IL1/IL1R1 signaling pathway in malignant tumors [51]. Among the ligands of IL1R1, IL1α enhances T cell-mediated antitumor immunity to suppress tumor growth, whereas IL1β stimulates tumor growth [52]. Silencing IL1R1 in AML contributes to a notable suppression of AML cell proliferation and cancer progression [53]. Similarly, we found that IL1R1 is a risk factor for AML and is correlated with a cold immune microenvironment. Thus, IL1R1 may be a potential target in AML. UCHL1 is a member of the UCH family of deubiquitinating enzymes (DUBs) and participates in many cellular processes, including cell cycle regulation, inflammatory responses, and oncogenesis [54]. Recently, UCHL1 was found to be highly expressed in carcinomas of various tissue origins and inhibited apoptosis and necroptosis to promote proliferation and invasion [55–57]. In line with these findings, our study revealed that UCHL1 expression is related to inferior clinical outcomes in patients with AML. In summary, our study established and verified a PANoptosis risk signature for predicting survival and the immunological treatment response in patients with AML.

5. Limitations and current perspectives

Our study had several limitations. For instance, we performed a signature analysis using transcriptome data from public databases; therefore, the sample data are limited. However, these results lacked experimental support. Additionally, because data on AML immunotherapy are deficient, the evaluation we performed was limited. Therefore, in future studies, we will conduct experiments and further investigations to explore the mechanisms of the PANoptosis risk signature in AML. Our study represents a significant advancement in the field of cell death. Through in-depth studies, we can better understand the molecular mechanisms and pathophysiology of AML.

6. Conclusions

The PANoptosis-risk signature could be an independent prognostic factor for AML. Three model factors including BIRC3, PELI1 and PRKACG are potential biomarkers for immunotherapy efficacy prediction in AML.

CRediT authorship contribution statement

Lu Zhang: Writing – original draft, Visualization, Software, Methodology, Formal analysis, Conceptualization. **Yanan Yu:** Validation, Software, Methodology, Formal analysis, Data curation. **Guiqing Li:** Methodology, Data curation. **Jiachun Li:** Investigation. **Xiaolin Ma:** Investigation. **Jiao Ren:** Investigation. **Na Liu:** Investigation. **Songyue Guo:** Investigation. **Jiaqiu Li:** Writing – review & editing, Supervision, Project administration, Funding acquisition, Conceptualization. **Jinwei Cai:** Supervision, Project administration.

Data availability statement

These data were derived from the following resources at TCGA-AML, GSE37642 and GSE12417.

Ethics declarations

Not applicable.

Funding

This work was supported by the Demonstration Project of Weifang Public Hospital Reform and High Quality Development, the National Natural Science Foundation of China (81902404), the Natural Science Foundation of Shandong Province (ZR2019BH009)

and the Project of Shandong Province medical science technology development plan (2017WS403).

Declaration of competing interest

The authors declare that they have no known competing financial interests or personal relationships that could have appeared to influence the work reported in this paper.

Acknowledgements

We acknowledge public databases for providing their datasets.

List of abbreviations

AML	acute myeloid leukemia
CyN	cyclic neutropenia
DUBs	deubiquitinating enzymes
GDSC	Genomics of Drug Sensitivity in Cancer
GEO	Gene Expression Omnibus
GO	Gene Ontology
G-CSF	granulocyte colony-stimulating factor
ICs	immune checkpoints
KEEG	Kyoto Encyclopedia of Genes and Genomes
K-M	Kaplan–Meier
LASSO	least absolute shrinkage and seletion operator
PRDEGs	PANoptosis-related differentially expressed genes
PDB	Protein Data Bank
PRGs	PANoptosis-related genes
PKA	protein kinase
SCN	severe congenital neutropenia
TCGA	The Cancer Genome Atlas
TIDE	Tumor Immune Dysfunction and Exclusion

Appendix A. Supplementary data

Supplementary data to this article can be found online at https://doi.org/10.1016/j.heliyon.2024.e40267.

References

[1] L. Bullinger, K. Dohner, H. Dohner, Genomics of acute myeloid leukemia diagnosis and pathways, J. Clin. Oncol. 35 (9) (2017) 934–946.
[2] S. Al-Harbi, et al., An update on the molecular pathogenesis and potential therapeutic targeting of AML with t(8;21)(q22;q22.1);RUNX1-RUNX1T1, Blood Adv 4 (1) (2020) 229–238.
[3] J. Prada-Arismendy, J.C. Arroyave, S. Röthlisberger, Molecular biomarkers in acute myeloid leukemia, Blood Rev. 31 (1) (2017) 63–76.
[4] P.B. Staber, et al., The Runx-PU.1 pathway preserves normal and AML/ETO9a leukemic stem cells, Blood 124 (15) (2014) 2391–2399.
[5] U. Höckendorf, et al., RIPK3 restricts myeloid leukemogenesis by promoting cell death and differentiation of leukemia initiating cells, Cancer Cell 30 (1) (2016) 75–91.
[6] P. Samir, R.K.S. Malireddi, T.D. Kanneganti, The PANoptosome: a deadly protein complex driving pyroptosis, apoptosis, and necroptosis (PANoptosis), Front. Cell. Infect. Microbiol. 10 (2020) 238.
[7] A.H.W. Hartmut Döhner, Frederick R. Appelbaum, Charles Craddock, Courtney D. DiNardo, Hervé Dombret, Benjamin L. Ebert, Pierre Fenaux, Lucy A. Godley, Robert P. Hasserjian, Richard A. Larson, Ross L. Levine, Yasushi Miyazaki, Diagnosis and management of AML in adults: 2022 ELN recommendations from an international expert panel, Blood (2022).
[8] L. Li, et al., Decitabine downregulates TIGAR to induce apoptosis and autophagy in myeloid leukemia cells, Oxid. Med. Cell. Longev. 2021 (2021) 8877460.
[9] Brumatti G, M.C., Lalaoui N, Nguyen NY, Navarro M, Tanzer MC, Richmond J, Ghisi M, Salmon JM, Silke N, Pomilio G, Glaser SP, de Valle E, Gugasyan R, Gurthridge MA, Condon SM, Johnstone RW, Lock R, Salvesen G, Wei A, Vaux DL, Ekert PG, Silke J., The caspase-8 inhibitor emricasan combines with the SMAC mimetic birinapant to induce necroptosis and treat acute myeloid leukemia. Sci. Transl. Med.
[10] S. Mao, et al., FLOT1 knockdown inhibits growth of AML cells through triggering apoptosis and pyroptosis, Ann. Hematol. 102 (3) (2023) 583–595.
[11] W. Yang, et al., Pyridoxine induces monocyte-macrophages death as specific treatment of acute myeloid leukemia, Cancer Lett. 492 (2020) 96–105.
[12] H. Wu, et al., Aprepitant sensitizes acute myeloid leukemia cells to the cytotoxic effects of cytosine arabinoside in vitro and in vivo, Drug Des. Dev. Ther. 14 (2020) 2413–2422.
[13] P. Stelmach, A. Trumpp, Leukemic stem cells and therapy resistance in acute myeloid leukemia, Haematologica 108 (2) (2023) 353–366.
[14] K. Bauer, et al., BRD4 degraders may effectively counteract therapeutic resistance of leukemic stem cells in AML and ALL, Am. J. Hematol. 99 (9) (2024) 1721–1731.
[15] P. Gui, T.G. Bivona, Stepwise evolution of therapy resistance in AML, Cancer Cell 39 (7) (2021) 904–906.
[16] S.K. Joshi, et al., The AML microenvironment catalyzes a stepwise evolution to gilteritinib resistance, Cancer Cell 39 (7) (2021) 999–1014.e8.
[17] D. Bertheloot, E. Latz, B.S. Franklin, Necroptosis, pyroptosis and apoptosis: an intricate game of cell death, Cell. Mol. Immunol. 18 (5) (2021) 1106–1121.
[18] N. Pandian, T.D. Kanneganti, PANoptosis: a unique innate immune inflammatory cell death modality, J. Immunol. 209 (9) (2022) 1625–1633.

[19] D.E. Place, S. Lee, T.D. Kanneganti, PANoptosis in microbial infection, Curr. Opin. Microbiol. 59 (2021) 42–49.
[20] W. Dan, et al., RIP1-dependent apoptosis and differentiation regulated by Skp2 and akt/GSK3beta in acute myeloid leukemia, Int. J. Med. Sci. 19 (3) (2022) 525–536.
[21] J. Xin, et al., Sensitizing acute myeloid leukemia cells to induced differentiation by inhibiting the RIP1/RIP3 pathway, Leukemia 31 (5) (2017) 1154–1165.
[22] X. Yu, et al., Overexpression of CASP1 triggers acute promyelocytic leukemia cell pyroptosis and differentiation, Eur. J. Pharmacol. 945 (2023) 175614.
[23] A.L. Nugues, et al., RIP3 is downregulated in human myeloid leukemia cells and modulates apoptosis and caspase-mediated p65/RelA cleavage, Cell Death Dis. 5 (8) (2014) e1384.
[24] D. Szklarczyk, et al., The STRING database in 2021: customizable protein-protein networks, and functional characterization of user-uploaded gene/measurement sets, Nucleic Acids Res. 49 (D1) (2021) D605–D612.
[25] S.Y. Park, Nomogram: an analogue tool to deliver digital knowledge, J. Thorac. Cardiovasc. Surg. 155 (4) (2018) 1793.
[26] J. Fu, et al., Large-scale public data reuse to model immunotherapy response and resistance, Genome Med. 12 (1) (2020) 21.
[27] P. Zhu, et al., Advances in mechanism and regulation of PANoptosis: prospects in disease treatment, Front. Immunol. 14 (2023).
[28] L.-X. Liu, et al., Sulconazole induces PANoptosis by triggering oxidative stress and inhibiting glycolysis to increase radiosensitivity in esophageal cancer, Mol. Cell. Proteomics 22 (6) (2023).
[29] R. Karki, et al., Interferon regulatory factor 1 regulates PANoptosis to prevent colorectal cancer, JCI Insight 5 (12) (2020).
[30] L. Zhuang, et al., A comprehensive analysis of PANoptosome to prognosis and immunotherapy response in pan-cancer, Sci. Rep. 13 (1) (2023).
[31] B. Zhang, et al., PANoptosis-related molecular subtype and prognostic model associated with the immune microenvironment and individualized therapy in pancreatic cancer, Front. Oncol. 13 (2023).
[32] J. Song, et al., The PANoptosis-related signature indicates the prognosis and tumor immune infiltration features of gliomas, Front. Mol. Neurosci. 16 (2023).
[33] X. Shi, et al., Construction of the panoptosis-related gene model and characterization of tumor microenvironment infiltration in hepatocellular carcinoma, Oncology Research 31 (4) (2023) 569–590.
[34] F. Song, et al., PANoptosis-based molecular subtyping and HPAN-index predicts therapeutic response and survival in hepatocellular carcinoma, Front. Immunol. 14 (2023).
[35] H. Pan, et al., Characterization of PANoptosis patterns predicts survival and immunotherapy response in gastric cancer, Clin. Immunol. 238 (2022).
[36] L. Tang, et al., Machine learning-based integrated analysis of PANoptosis patterns in acute myeloid leukemia reveals a signature predicting survival and immunotherapy, Int. J. Clin. Pract. 2024 (2024) 1–25.
[37] J. Zhang, et al., Transcriptome-based network analysis unveils eight immune-related genes as molecular signatures in the immunomodulatory subtype of triple-negative breast cancer, Front. Oncol. 10 (2020).
[38] K. Lyu, et al., Development and clinical validation of a necroptosis-related gene signature for prediction of prognosis and tumor immunity in lung adenocarcinoma, Am. J. Cancer Res. 12 (11) (2022) 5160–5182, 2022.
[39] R. Frazzi, BIRC3 and BIRC5: multi-faceted inhibitors in cancer, Cell Biosci. 11 (1) (2021) 8.
[40] P.Y. Fu, et al., New insight into BIRC3: a novel prognostic indicator and a potential therapeutic target for liver cancer, J. Cell. Biochem. 120 (4) (2019) 6035–6045.
[41] C.J. Hess, et al., Activated intrinsic apoptosis pathway is a key related prognostic parameter in acute myeloid leukemia, J. Clin. Oncol. 25 (10) (2007) 1209–1215.
[42] H. Wang, et al., PELI1 functions as a dual modulator of necroptosis and apoptosis by regulating ubiquitination of RIPK1 and mRNA levels of c-FLIP, Proc. Natl. Acad. Sci. U. S. A. 114 (45) (2017) 11944–11949.
[43] L. Zhang, et al., Peli1 facilitates NLRP3 inflammasome activation by mediating ASC ubiquitination, Cell Rep. 37 (4) (2021) 109904.
[44] D. Capece, et al., NF-kappaB: blending metabolism, immunity, and inflammation, Trends Immunol. 43 (9) (2022) 757–775.
[45] S. Mirzaei, et al., NF-kappaB as a regulator of cancer metastasis and therapy response: a focus on epithelial-mesenchymal transition, J. Cell. Physiol. 237 (7) (2022) 2770–2795.
[46] L. Li, Z.T. Zhang, Genetic association between NFKBia and NFKB1 gene polymorphisms and the susceptibility to head and neck cancer: a meta-analysis, Dis. Markers 2019 (2019) 6523837.
[47] M. Molgora, et al., TREM2 modulation remodels the tumor myeloid landscape enhancing anti-PD-1 immunotherapy, Cell 182 (4) (2020) 886–900, e17.
[48] F. Zhu, et al., Identification of key genes and pathways associated with RUNX1 mutations in acute myeloid leukemia using bioinformatics analysis, Med. Sci. Mon. Int. Med. J. Exp. Clin. Res. 24 (2018) 7100–7108, 2018.
[49] H. Kambara, et al., Gasdermin D exerts anti-inflammatory effects by promoting neutrophil death, Cell Rep. 22 (11) (2018) 2924–2936.
[50] X. Wang, X. Liu, H. Wang, Combination regimen of granulocyte colony-stimulating factor and recombinant human thrombopoietin improves the curative effect on elderly patients with leukemia through inducing pyroptosis and ferroptosis of leukemia cells, Cancer Gene Ther. 29 (11) (2022) 1742–1750.
[51] S.E. Acuner Ozbabacan, et al., The structural pathway of interleukin 1 (IL-1) initiated signaling reveals mechanisms of oncogenic mutations and SNPs in inflammation and cancer, PLoS Comput. Biol. 10 (2) (2014) e1003470.
[52] T. Tian, et al., IL1alpha antagonizes IL1beta and promotes adaptive immune rejection of malignant tumors, Cancer Immunol. Res. 8 (5) (2020) 660–671.
[53] A. Carey, et al., Identification of interleukin-1 by functional screening as a key mediator of cellular expansion and disease progression in acute myeloid leukemia, Cell Rep. 18 (13) (2017) 3204–3218.
[54] E. Matuszczak, et al., Ubiquitin carboxy-terminal hydrolase L1 - physiology and pathology, Cell Biochem. Funct. 38 (5) (2020) 533–540.
[55] S. Zheng, et al., Heterogeneous expression and biological function of ubiquitin carboxy-terminal hydrolase-L1 in osteosarcoma, Cancer Lett. 359 (1) (2015) 36–46.
[56] S. Hussain, et al., The de-ubiquitinase UCH-L1 is an oncogene that drives the development of lymphoma in vivo by deregulating PHLPP1 and Akt signaling, Leukemia 24 (9) (2010) 1641–1655.
[57] S.Y. Kwan, et al., Ubiquitin carboxyl-terminal hydrolase L1 (UCHL1) promotes uterine serous cancer cell proliferation and cell cycle progression, Cancers 12 (1) (2020).